



HAL
open science

How do organic polysulphides improve the performance of Li-S batteries?

Satyajit Phadke, Julie Pires, Alexander Korchenko, Mérièm Anouti

► To cite this version:

Satyajit Phadke, Julie Pires, Alexander Korchenko, Mérièm Anouti. How do organic polysulphides improve the performance of Li-S batteries?. *Electrochimica Acta*, 2020, 330, pp.135253 -. 10.1016/j.electacta.2019.135253 . hal-03488415

HAL Id: hal-03488415

<https://hal.science/hal-03488415>

Submitted on 21 Dec 2021

HAL is a multi-disciplinary open access archive for the deposit and dissemination of scientific research documents, whether they are published or not. The documents may come from teaching and research institutions in France or abroad, or from public or private research centers.

L'archive ouverte pluridisciplinaire **HAL**, est destinée au dépôt et à la diffusion de documents scientifiques de niveau recherche, publiés ou non, émanant des établissements d'enseignement et de recherche français ou étrangers, des laboratoires publics ou privés.



Distributed under a Creative Commons Attribution - NonCommercial 4.0 International License

How do organic polysulphides improve the performance of Li-S batteries?

Satyajit Phadke^a, Julie Pires^a, Alexander Korchenko^b, and Mérièm Anouti^{a}*

^a *Laboratoire PCM2E, Université de Tours, Parc de Grandmont, 37200, Tours, France*

^b *ARKEMA, Groupement de Recherches de Lacq, 64170, Lacq, France*

Corresponding author: meriem.anouti@univ-tours.fr

Abstract

Lithium-sulphur (Li-S) batteries are promising energy storage systems, but it suffers from several limitations mainly due to the electrolytes. In this study, we explore the effect of organic sulphides on the modification of the system performance of Li-S. We compare in this study, the effect of catholytes based on three differently functionalized organic sulphides as models. These include an activated thiol (tri-fluoro methane benzene thiol: BTFBT) (1), a weakly activated aromatic disulphide (diphenyl disulphide: Ph₂S₂) (2) and a di-thiol deactivated by a di-ether function: DMDO) (3). The galvanostatic discharge profile of sulphur based-cathode exhibits an additional first plateau corresponding to the electrochemical redox voltage of the disulphide (or thiol) initially present in the catholyte. Their reduction voltage (vs. Li⁺/Li) follows the order BTFBT > S₈ ≈ Ph₂S₂ > DMDO and is directly dependent on the electron withdrawing/donating nature of the organic sulphide. The presence of the organic sulphide in the catholyte increases the capacity utilization of mineral sulphur of the cathode by approximately 33.8%, 49.3% and 27.9% in case of BTFBT, DMDO and Ph₂S₂ respectively at a C-rate of C/5. To explain these observations, we propose potential chemical balance between the redox systems (S₈/S_x²⁻) and (RS_xR / RS_x⁻) in the solution kinetically and thermodynamically controlled. Furthermore, the lithium anode behaviour was also probed by lithium stripping/deposition measurements. Results indicate that the presence of 0.2 M Ph₂S₂ in the catholyte increases the overvoltage by ~32 mV due to deposited of stable protective lithium thiolate layer as observed by SEM. Finally, long term cycling of 500 cycles validates the positive effect of the organic catholytes as chemical barrier against sulphur loss during cycling.

Keywords: Lithium-sulphur batteries, catholyte, organic sulphides, high capacity

1. Introduction

Energy storage devices and particularly Lithium-ion batteries are rapidly gaining importance due to the sustained growth in the electronic devices sector and the growing need for electric vehicles (EVs).[1] For these applications, the energy density (Wh.kg^{-1}) of the batteries is a critical parameter for weight reduction of electronic devices and for extending the driving range of EVs in order to prevent ‘range anxiety’[2]. As a result, Lithium-sulphur (LiS) batteries, which have a potential for achieving higher energy density are globally under research focus.[3-5] This is primarily due to the high theoretical specific capacity of mineral sulphur (1672 mAh.g^{-1}) and metallic lithium (3862 mAh.g^{-1}) which translates to a theoretical energy density of 2260 Wh.kg^{-1} . [6]

However, two fundamental challenges concerning the sulphur cathode need to be overcome in order to realize the full potential of the technology. It is now widely established that lithium salts with long chain polysulfide ions are much more soluble than short chain ones. In addition, the short chain polysulphides have an insulating nature that is harmful to the performance of the battery. [7-12] On this topic, most approaches in literature focus on the development of microscopically architected materials targeted at confining the soluble species formed during the electrochemical redox reactions and limiting their long-range diffusion.[13-17] The use of highly concentrated electrolytes, solid polymer electrolyte (SPE) or ceramic ion conducting electrolytes has also been demonstrated to be an effective strategy in mitigating the challenges associated with polysulphide dissolution.[18-20] However, these complex electrode modification approaches often involve a compromise on the energy density due to the large weight fraction of conductive additives and host structures required.[3] On the other hand, due to the low ionic conductivity and high interfacial resistance of the solid electrolytes, high c-rate capability is often restricted and energy efficiency is reduced.[21]

There are relatively few studies focusing on the modification of the electrolyte by comparison with cathode modification to address the challenges associated with performance and capacity retention of Li-S batteries. The functional electrolytes or catholytes for Li-S batteries explored in this study can alleviate the problems Li-S batteries face today, especially relating to the fundamental polysulfide shuttle mechanism. Recently, some studies were published focusing on different functional solvents, lithium salts and additives to improve the surface of the lithium anode [22-24] or to increase the conductivity of the electrolyte [25-29]. However, none of these constitute a real solution to the chemical

reactivity of sulphur and polysulphide ions, which remains the major problem of Li-S batteries.

We have recently published a work based on the principle of using organic polysulfide as a chemical barrier to the redox shuttle of LiS batteries focusing on the use of diphenyl disulphide (Ph_2S_2).[30] . This approach is quite new to the LiS community with only a few publications up to now.[31, 32]. To complete this work, we present herein, a comparative study of the impact of catholytes containing electrochemically active organic disulphide (R_2S_2), thiol (RSH) or dithiol (SHRSH) compounds on the discharge capacity and capacity fade rate of the sulphur cathode in LiS batteries. The goal of this study is to understand the underlying mechanisms and to explain the role of the organic polysulfide in suppression of the shuttle effect. We present firstly, the fundamental considerations that will help understand the many complex chemical and electrochemical interactions between inorganic ($\text{S}_8/\text{S}_x^{2-}$) and the organic ($\text{RS}_x\text{R}/\text{RS}^-$) systems. We will then compare the role of each compound in improving observed performance.

2. Fundamental considerations

Reduction of the mineral sulphur in the cathode occurs via a multistep process.[33] The profile of first discharge for C/S cathode in the reference electrolyte (DOL/DME (1:1, v) + 0.75 M LiTFSI + 0.25 M LiNO_3) is shown in Figure 1. This typical profile[34-36] is characterized by two plateaus P_1 (~2.38 V vs Li^+/Li) and P_2 (~2.05 V vs Li^+/Li) and two sloping regions (R_1 , R_2) corresponding to theoretical capacity of 209, 420, 1250 and 1675 mAh.g^{-1} as ideally showed by discharge curve in Figure 1.

In fact, during cycling the mineral sulphur/polysulfide redox system generates a series of ion intermediates directly resulting from the electrochemical solid/liquid or the liquid/liquid reduction (Table 1) or by the complicated disproportionation and exchange reactions (Table 2). The first step is the reduction of the elemental sulphur (S_8) to S_8^{2-} , followed by its reduction to (S_3^{2-} , S_4^{2-}) and subsequently to short chain polysulphides (S_2^{2-} , S^{2-}). The generated lithium polysulfides (i.e ($2\text{Li}^+, \text{S}_x^{2-}$), $1 < x \leq 8$) consists of high solubility long chain species (S_x^{2-} ; $x \geq 4$) resulting in an uncontrollable diffusion in cells. On the other hand, the short chain species (S_x^{2-} ; $x \leq 2$) precipitate out as Li_2S_x causing irremediable loss of

reducible sulphur. The electrochemical and chemical balance reactions for (S/S_y^-) system, are summarized in Table 1 and Table 2 respectively.

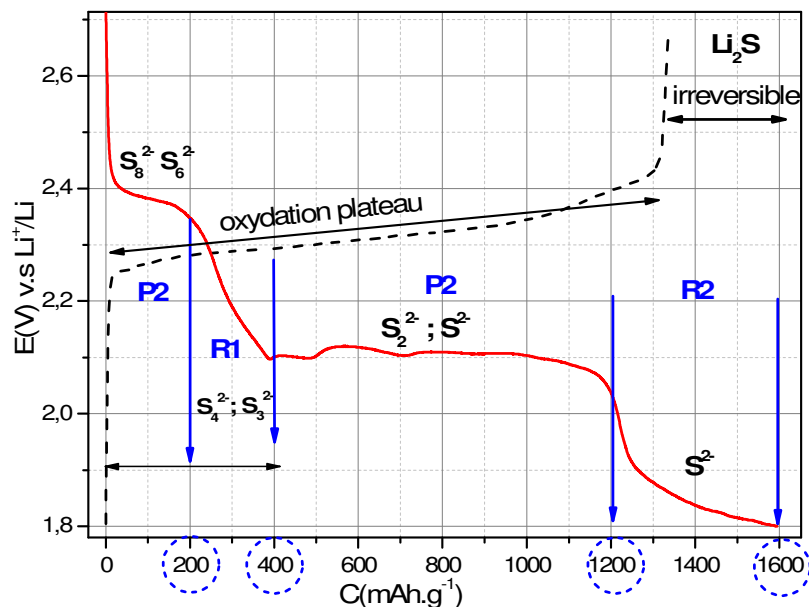


Figure 1. First discharge charge profile of C/S cathode in DOL/DME (1:1, w) + 0.75M LiTFSI + 0.25M LiNO₃ at C/20 visualising the different plateaus (P_i) and sloping regions (R_i) and showing the major reaction products at each step according mechanism listed in Table 1.

In the first plateau (P₁), a solid-liquid two-phase electrochemical reaction occurs, corresponding to the opening of the octa-sulphur (S₈) molecules and its subsequent reduction to S₈²⁻. These species migrate out of the cathode via diffusion and electrical drag in electrical field (transport) and are subject to several chemical reactions as exchange (Eq. 5 in Table 2) and dissociation of radical anions (Eq. 6 and Eq. 7 in Table 2). In presence of lithium cations, the high soluble salts Li₂S₈, Li₂S₆ migrate, diffuse and react without solubility limitation. The competition between the electrochemical process (Eq. 1, 2) and the kinetically controlled chemical steps (Eq. 5-7) largely depend on the electronically conductive nature of the cathode (electron transfer Eq. 1-2) and the ability of the solvent to promote “thiophilicity” (Eq. 5) and dimerization (Eq. 6-7). Overall, the first plateau corresponds to the complete reduction of the sulphur of the electrode to the dimers S₆²⁻ and S₈²⁻, in balance with their radical-anions S₃⁻

and S_4^{2-} . The electronic balance of this step corresponds to $2e^-$ for $8S$ and reaches 200 mAh.g^{-1} of S .

Table 1. Electrochemical reactions involved in the different stages of sulphur reduction. Major product in the mixtures, and specific capacity at the end of each step.

Eq	Step or balance	Electrochemical reaction	Major Product	Theoretical C_{sp} (mAh.g^{-1})	Balance (mAh.g^{-1})
(1)	First Plateau (P ₁)	$S_8 + 2 e^- \rightarrow$	S_8^{2-}	209	
(2)	Slop region (R ₁)	$S_8^{2-} + 2 e^- \rightarrow$	$2 S_4^{2-}$	209	
Balance 1	(1) + (2)	$S_8 + 4 e^- \rightarrow$	$2 S_4^{2-}$	419	419
(3)	Second Plateau (P ₂)	$2 S_4^{2-} + 8 e^- \rightarrow$	$2 S_2^{2-} + 4 S^{2-}$	839	
Balance 2	(1) + (2) + (3)	$S_8 + 12 e^- \rightarrow$	$4 S_2^{2-}$	1259	1259
(4)	slope region (R ₂)	$2 S_2^{2-} + 4 e^- \rightarrow$	$4 S^{2-}$	419	
Balance 3	(1) + (2) + (3) + (4)	$S_8 + 16 e^- \rightarrow$	$4 S^{2-}$	1678	1678

The second part of the discharge curve is a sloping region. It corresponds to the competitive and simultaneous reduction of the two species from the first stage. At the same time, the disproportionation reactions of the two anions (S_4^{2-} and S_3^{2-}) transform this step into a superposition of small plateaus (sloping region). We can calculate the theoretical capacity of this step similar to the first step. An extraction of sulphur and its total reduction made possible by the sufficiently slow rate ($C/20$), ensures that the entire theoretical capacity of 400 mAh.g^{-1} is obtained at the end of the first two stages.

Table 2. Chemical reactions involved in the different stages of sulphur reduction. Composition of the mixtures at the end of each step.

Step	Eq.	Reaction nature	Chemical reaction	Major Product	Control	Mixture at the end step
P1	(5)	exchange	$S_8^{2-} + \frac{1}{4} S_8 \rightarrow$	S_6^{2-}	$K_5 ; k_5$	$S_8^{2-} ; S_6^{2-}$

	(6)	dissociation	S_8^{2-}	\rightarrow	$2 S_4^{2-}$	$K_6,$ fast	$S_3^{2-}; S_4^{2-}$
	(7)	dissociation	S_6^{2-}	\rightarrow	$2 S_3^{2-}$	$K_7,$ fast	
R1	(8)	disproportionation	$3S_4^{2-}$	\rightarrow	$2S_3^{2-} +$ S_6^{2-}	$K_8 ;$ k_8	$S_3^{2-}; S_4^{2-};$ S_6^{2-}
P2	(9)	disproportionation	$2S_2^{2-}$	\rightarrow	$S_3^{2-} +$ S^{2-}	$K_9 ;$ k_9	$S_3^{2-}; S_2^{2-};$ S^{2-}
R2	(10)	Exchange	$2S^{2-}$ $2S_3^{2-}$	$+$ \rightarrow	S_2^{2-}	$K_{10} ;$ k_{10}	$S_2^{2-}; S^{2-}$

When the potential is sufficiently low to oppose their disproportionation ($E = 2.1$ V vs Li^+/Li), the S_4^{2-} ions are reduced in a single di-electronic step (Eq. 3) to disulphide ions S_2^{2-} . These much more reductive and much more mobile ions diffuse rapidly in solution towards the anode. The outcome of this step will again depend on the competition between (i) the ion diffusion rate, (ii) the electron transfer rate and (iii) the rate of their own chemical disproportionation. Furthermore, the effective protection of the anode against the deposition of poorly soluble Li_2S_2 salts can modify the quantitative issue of this step. This step consumes $8e^-$ for $8S$ ($2S_4^{2-}$) and has a balance of 800 $mAh.g^{-1}$. In fact, the ratio between the plateau P_1 , region R_1 and plateau P_2 is ideally $r = \frac{P_2}{(P_1+R_1)} = 2$. Any decrease in this ratio will indicate a loss of reactive species by salt precipitation (Li_2S or Li_2S_2) or their electrochemical inactivity due to unevaluable protection of anode (Li metal) by $LiNO_3$ salt.

At this stage of the reduction of the cathode, the overall balance is 1200 $mAh.g^{-1}$. This is the effective part of the charge that can be stored reversibly in the C/S electrode. Beyond the plateau P_2 , only the ions S_2^{2-} remain in solution. Their electrochemical reduction leads to strongly reducing S^{2-} ions accompanied by their high chemical reactivity and their precipitation in the form of Li_2S salts. This step consumes an equivalent amount of current that the balance ($P_1 + R_1$, i.e 400 $mAh.g^{-1}$), and its sloping form is synonymous with the superposition of chemical/electrochemical processes. In summary, as shown on the Figure 1, the reduction of sulphur can be schematically divided into 3 regions of ($P_1 + R_1$); P_2 ; R_2 whose ratios are proportional, equal to 2, 1, and 1, respectively. The ratios: $r_1 = \frac{P_1}{R_1}$; $r_2 = \frac{P_2}{(P_1+R_1)}$; $r_3 = \frac{P_2}{R_2}$ provide information on the competition of the reactions (E) v.s (C) and therefore depend on the material (E) and the electrolyte (C) (diffusion); Ideally $r_1 = 1$; $r_2 = 2$; $r_3 = 2$. The irreversible part of total capacity is due to the loss of part of sulphur as Li_2S and is linked to the plateau R_2 region and corresponds to precipitated Li_2S .

In low C-rate conditions (C/20), at oxidation, a large part of the sulphur in solution is redeposited in a single step on the carbon matrix of the cathode (1300 mAh.g⁻¹). Only Li₂S inaccessible to oxidation, lack in the balance C_{Dis}/C_{Ch} = 80% and corresponds to the irreversible. Each of the stages P1, R1, P2 and R2 sulphur of the competition of the chemical and electrochemical reactions and remains totally related to various factors (chemical balance, electronic transfer at the cathode, effective anode protection toward dendrites end passivation). In fact, the discharge regime (C/n) reflect theses parameters and completely changes the curve shape or electrochemical balance for each region.

The presence of the organic sulphur (thiol, disulphide) in the electrolyte introduces a new redox system (R₁S_nR₂/RS⁻, R₁, R₂ = alkyl, aryl, or H; n = 1,2) in addition to the existing redox of mineral sulphur in the cathode (S₈, S_x²⁻). All inorganic and organic sulphur compounds are selectively reducible and oxidizable at potential determined by their electronic properties, the interface of the electrodes[37]. Moreover, all the species present interact in chemical equilibria thermodynamically (K_i), and kinetically (k_i) controlled as summarised by table 3.

Table 3. Chemical reactions involved in the different stages of thiol, dithiol or disulphide additive. Composition of the mixtures at the end of each step.

System	Eq	Reaction nature	Chemical reaction	Major Product	Control	Mixture at the end step
Thiol / Thiolate or Dithiol/dithiolate	(11)	Reduction (E)	2RSH + 2 e ⁻ →	2RS ⁻ + H ₂	K ₅ ; k ₅	S, RS _z R RS _y ⁻ ; S _x ²⁻
	(12)	Reduction (Li ⁰)	2RSH + S _x ²⁻ →	2RS ⁻ + H ₂	k ₅	(2 ≤ x ≤ 8)
	(13)	Redox (E)	2RS ⁻ - 2 e ⁻ ⇌	RS ₂ R	k ₅	(1 ≤ y ≤ 5) (2 ≤ z ≤ 4)
	(14)	Exchange	S _x ²⁻ + RS ₂ R →	2RS ⁻ + x S [·]	K ₁₁	
Disulphide/ thiolate	(15)	Thiophilicity	RS ⁻ + y S [·] →	RS _y ⁻	K ₅ ; k ₅	
	(16)	Oxidation (E)	2RS _y ⁻ - 2 e ⁻ →	RS ₂ R + (y-z) S	K ₅ ; k ₅	
	(13)	Redox (E)	RS ₂ R + 2 e ⁻ ⇌	2RS ⁻	K ₅ ; k ₅	S, RS _z R RS _y ⁻ ; S _x ²⁻
Disulphide/ thiolate	(15)	Thiophilicity	RS ⁻ + y S [·] →	RS _y ⁻	K ₅ ; k ₅	
	(14)	Exchange	S _x ²⁻ + RS ₂ R →	2RS ⁻ + x S [·]	K ₉ ; k ₉	(2 ≤ x ≤ 8) (1 ≤ y ≤ 5)
	(16)	Oxidation (E)	2RS _y ⁻ - 2 e ⁻ →	RS ₂ R + (y-z) S	K ₁₀ ; k ₁₀	(2 ≤ z ≤ 4)

In aprotic media, the issue of electrochemical reduction of thiols and disulphides (eq 10 and eq 13, table 3) is the thiolate ion RS^- [38]. Its stabilization depends on (i) the charge delocalisation of the sulphur atom, due to the neighbouring electronic effects), (ii) its reactivity as a nucleophile called "thiophilicity". In same time both disulphide and thiol react instantaneously with the chemical reducers polysulphides ions, to produce thiolate (eq 12 and eq 14) [39-44]. This chemical reactivity between (S/S_x^{2-}) and (RS_xR/RS^-) redox systems were evidenced by spectroelectrochemistry (ref) and correspond to the successive steps: (i) initial exchange equilibria (eq 14) (ii) concurrent thiophilicity of the thiolate ions toward sulfur (eq 15), as established by direct addition of sulfur to thiolate ions by Anouti *et. al.* [45-48]. The relative reducing power of the polysulfide ions ($S_8^{2-} < S_4^{2-} < S_2^{2-}$) and the breaking capacity of the S-H or S-S bond in RSH and RSSR, will depend on the displacement (K_i) and kinetic (k_i) of the mentioned redox equilibria.

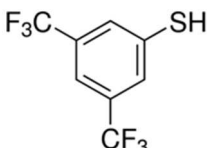
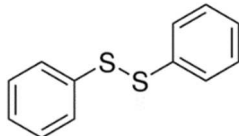
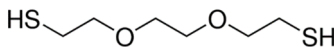
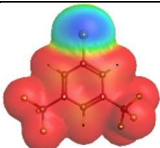
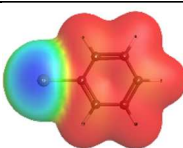
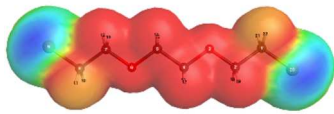
The three electrolyte additives considered in this study are diphenyl-disulphide (Ph_2S_2), (3,5)-bis (tri-fluoromethyl) benzene thiol (BTFBT) and (2,2')-(Ethylenedioxy) diethane thiol (DMDO). The structure and chemical formula of the compounds are listed in Table 4. In the absence of a catalyst, reduction of disulphide is electrochemically irreversible with a large gap (~ 1.5 V) between the reduction and oxidation potential ($E_{Ox} - E_{Red}$) depending to the structure nature.[49, 50] The reduction potential, thiophilicity and exchange equilibrium are strongly dependent on the nature of R as shown by Anouti *et. al.* [45-48]²³⁻²⁶.

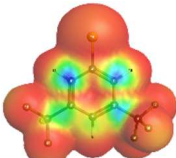
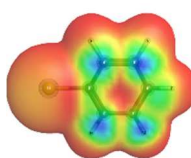
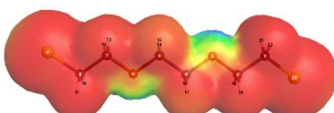
The three chosen organic disulphide compounds for this study, exhibit widely distinct structural, electronic and functional properties of the R group. The negative charge on sulphur in the thiolate decreases as the electron withdrawing nature of the R increases. A strongly electron withdrawing nature as in case of $R = (CF_3)_2PhS^-$ due to the presence of two $-CF_3$ groups attached to the phenyl ring, allows the negative charge on the sulphur atom to be distributed more effectively. To compare the relative stability of the three compounds studied here, we calculated by molecular modelling (Ab-initio with the MOPAC semi-empirical method) the partial charge on the sulphur atom as well as the energy levels of the HOMO, LUMO boundary orbitals for thiolate ions (RS^-) where $R = (CF_3)_2PhS^-$, PhS^- and $(CH_2O(CH_2)_2S^-)_2$. are summarized in Table 4. These values give an indication about their comparative nucleophilicity [51]and also their tendency to oxidize (HOMO) [52-54].

The charge seems much more localized on the sulphur ($\delta = - 0.9$) in the case of the DMDO because of the pronounced donor effect. This at the same time renders this species easier to

oxidize (HOMO) and potentially more nucleophilic. On the contrary, in BTFBT due to the presence of the two-electron attracting $-\text{CF}_3$ groups, the localized charge on sulphur (-0.69) is minimized consequently presenting the most stable thiolate ion. It is therefore possible to expect a lower chemical (nucleophilicity) and electrochemical (oxidation) reactivity of CF_3PhS^- ions compared to the other two ions. By sequencing the chemical or electrochemical reduction of the corresponding disulphide or thiol would be easier $(\text{CF}_3)_2\text{PhS}^- > \text{PhS}^- > (\text{CH}_2\text{O}(\text{CH}_2)_2\text{S}^-)_2$. The PhS^- having an intermediate position in terms of sulphur charge ($\delta = -0.78$) and HOMO level could be expected to have intermediate properties.

Table 4. Name, structure, theoretical and normalized (as per weight of mineral sulphur) specific capacity for Thiol, dithiol and disulphide. Calculated sulfur charge, HOMO and LUMO orbital energies for thiolates via MOPAC semi-empirical calculation are also reported

Name (Abbreviation)	Bis (trifluoro methyl) benzene thiol (BTFBT)	Diphenyl disulphide (Ph_2S_2)	Ethylene dioxy diethanethiol (DMDO)
Category	Thiol (R-SH)	(Di-sulphide (R-S-S-R	Di-thiol (HS-R-SH)
Structure			
Theoretical Specific Capacity (mAh.g ⁻¹)	109	246	295
Specific Capacity (mAh.g ⁻¹) normalized by S mass on cathode ^(a)	2086	2508	2280
Ratio S(cathode)/ S(electrolyte)	0.25	0.5	0.31
Thiolate/ Dithiolate ions	$(\text{CF}_3)_2\text{PhS}^-$	PhS^-	$(\text{CH}_2\text{O}(\text{CH}_2)_2\text{S}^-)_2$
HOMO orbital			

LUMO orbital			
Charge of S	-0.69	-0.75	-0.90
HOMO (eV)	-3.95	-3.06	-1.27
LUMO (eV)	+2.95	+4.51	+7.27

^(a) Total theoretical normalized capacity by mass of mineral sulphur in the cathode. $C_S = 1678$ mAh.g⁻¹ for cathode without organic thiolate in catholyte.

On the other hand, the electrochemical reduction of these sulphur-containing organic compounds generates an additional capacity proportional to their molar mass. From this point of view, DMDO has the greatest advantage due to its low mass. With nearly 300 mAh.g⁻¹, it generates three times more capacity than the BTFBT. It is however important when calculating the additional capacity to consider the ratio of mineral sulphur (introduced by the electrode) and organic sulphur contained in the electrolyte. It is then possible to standardize the calculation of the capacity with respect to the sulphur mass in the electrode considering this ratio. Only this method allows correct comparison of a C/S cathode cycling behaviour with and without additive. In Table 4, we summarize, name, chemical formula, theoretical and normalized specific capacity for organic polysulphides additives considered in this study. The calculated sulfur charge, HOMO and LUMO orbital energies of the respective thiolates via MOPAC semi-empirical calculation are also listed.

3. Experimental Procedure

3.1. Electrode preparation

The sulphur/CNT blend mixture was thoroughly mixed in the weight ratio 2:1 with carbon additive (Ketjen Black, EC-600JD) in a mortar and pestle to form a uniform powder mixture. Separately, 5 wt% of PVDF was dissolved into NMP to prepare a solution. An appropriate quantity of this solution was added to the powder mixture and kept under magnetic stirring for approximately 1 h to produce a homogeneous ink. The overall weight ratio of the S:C:PVDF in the ink was 6:3:1. The ink was painted on pre-cut discs (14 mm dia.) of graphite paper (Sigracet BC, SGL Carbon) and dried under vacuum at 90°C for 3 h. The

dried electrodes were directly taken into the glovebox without exposure to ambient air. The average loading of sulphur on the electrode was $1.2 - 1.5 \text{ mg.cm}^{-2}$.

3.2. Electrolyte formulation

The standard reference electrolyte was prepared by mixing solvents 1,3 Dioxolane (DOL) (Sigma Aldrich, 99.9) and 1,2 Dimethoxyethane (DME) (Sigma Aldrich, 99.9) in a volume ratio of 1:1. To this solvent mixture, 0.75 M LiTFSI (Sigma Aldrich, 99.95%) and 0.25 M LiNO₃ (Sigma Aldrich, 99.99%) were added and dissolved by magnetic stirring. To prepare the catholytes containing 0.2 M disulphide, thiol or di-thiol, a measured weight of the relevant compound was added to the standard electrolyte. The disulphides and thiols are readily soluble in the electrolyte. In this study, the LiS cells are sealed using different catholytes with 0.2 M electrochemically active compound concentration. These catholytes or cells containing them are referred to simply by the name of the organic sulphide added namely Ph₂S₂, BTFBT or DMDO. An electrolyte containing no organic sulphide is referred to as the standard electrolyte.

The ratio of sulphur in cell is related to the amount of sulphur in the electrode (1.2 mg to 1.5 mg) with 1678 mAh.g⁻¹ of theoretical capacity and the amount of sulphur in organic additives (RS₂R, or RSH) which provide additional capacity (see table 4). These theoretical capacities have been normalized with respect to the sulphur mass in the electrode in order to be able to compare all the samples. In our experimental conditions (100 μL of electrolyte, 0.2 mol. L⁻¹) and (1.2 – 1.5) mg.cm⁻² of S/cathode) the ratio S (electrolyte) / S (electrode) is respectively 25%, 30% and 50% for BTFBT, DMDO and Ph₂S₂.

3.3. Electrochemical Testing

For electrochemical testing, coin cells (CR 2032) were assembled using the prepared sulphur electrodes as cathode and Lithium foil (Sigma Aldrich, 99.9%, 0.75 mm thickness) as the anode. Two pre-cut discs (16 mm dia.) of Whatmann separator (GF/C) were inserted between the anode and the cathode. Prior to cell sealing, 100 μL of electrolyte (carefully measured via micropipette) was dropped on the separator ensuring no spillage outside the cell. All steps involving the cell fabrication were performed inside an atmosphere-controlled glovebox where the H₂O and O₂ concentration was maintained below 0.1 ppm. Potential limits of 2.7 V – 1.8 V were used for all galvanostatic testing. Galvanostatic cycling was carried out using a VMP multichannel potentiostatic/galvanostatic system (Biologic Science Instrument, France).

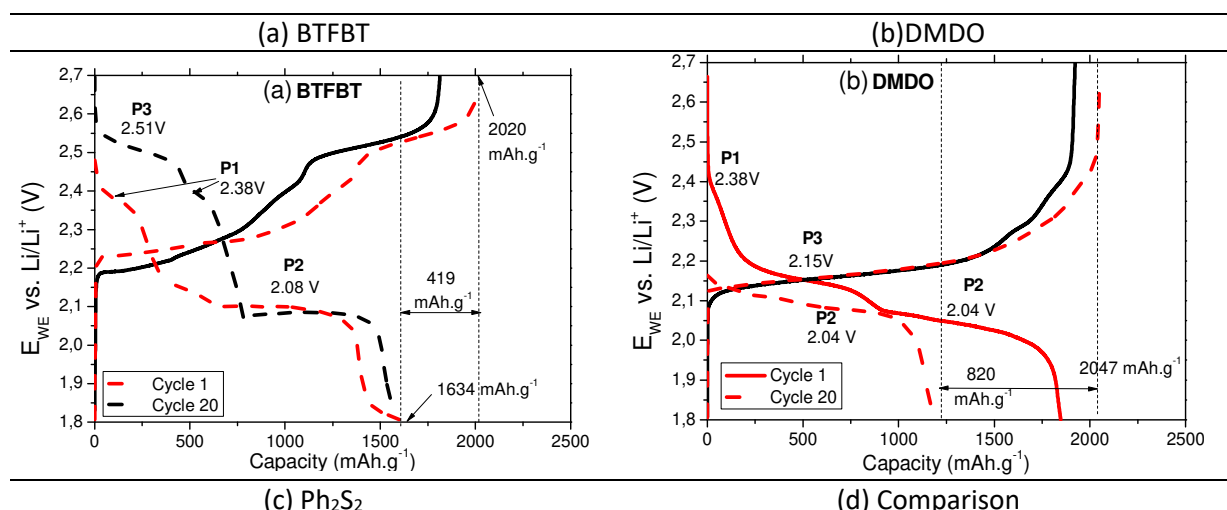
For Lithium stripping /deposition measurements, two symmetric Lithium electrodes (10 mm dia.) were placed in the coin cell separated by a Whatmann separator. The surface of the lithium was scratched before cell assembly. Prior to cell sealing, 100 μL of the appropriate electrolyte was added. A current density of 0.4 mA.cm^{-2} was used for cycling with a 20-minute interval for changing the current direction. After the measurement, the cell was opened inside the glovebox and the Lithium electrode was washed and stored in a vial containing DOL. The Scanning Electron Microscope (SEM) images were obtained using a Zeiss ultra+ equipped with a secondary electron sensor.

4. Results and Discussion

4.1. Effect on the First discharge (C/10)

Figure 2 shows the galvanostatic profiles of a C/S cathode (cycle 1 and cycle 20) at C/10 for the cells with catholytes containing 0.2 mol.L^{-1} of (a) BTFBT, (b) DMDO and (c) Ph_2S_2 . The addition of the organic sulphide in the catholyte modifies voltage profile significantly due to the observance of an additional plateau P3. The exact voltage for P3 corresponds to the reduction voltage of thiol, dithiol or disulphide. This in turn depends strongly on the nature of the organic sulphide, the ability of S—S bond breakage and thiolate ion stabilisation.

A similar relationship between the reduction potentials and nature of R has been reported previously for a different set of organic disulphides.[50]. This additional step adds a capacity that can be related to the active sulphur mass in the cathode for comparison as discussed previously and reported in Table 4. The calculated theoretical normalized capacity for the cells without and with BTFBT, DMDO and Ph_2S_2 was 1678, 2086, 2280, 2508 mAh.g^{-1} of S in cathode respectively.



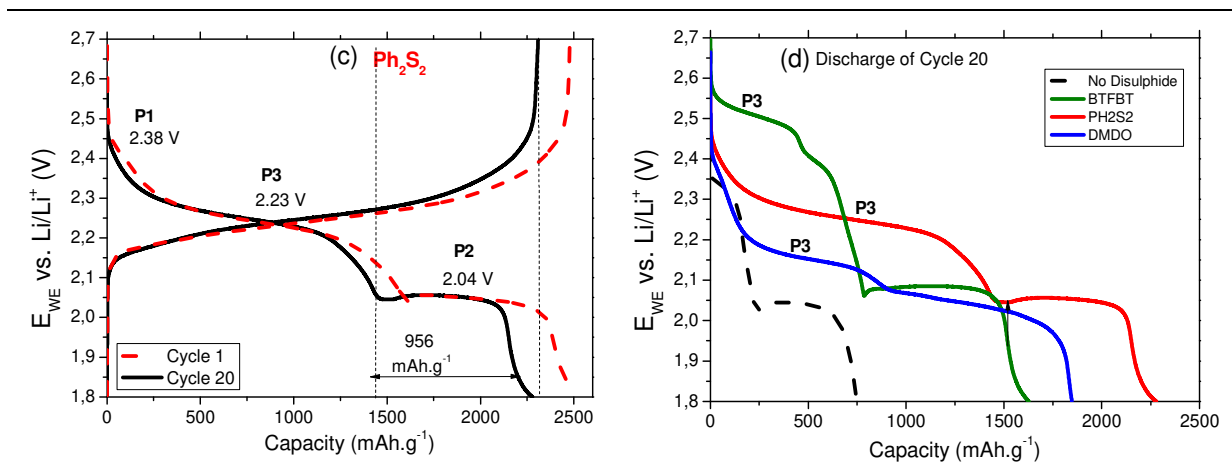
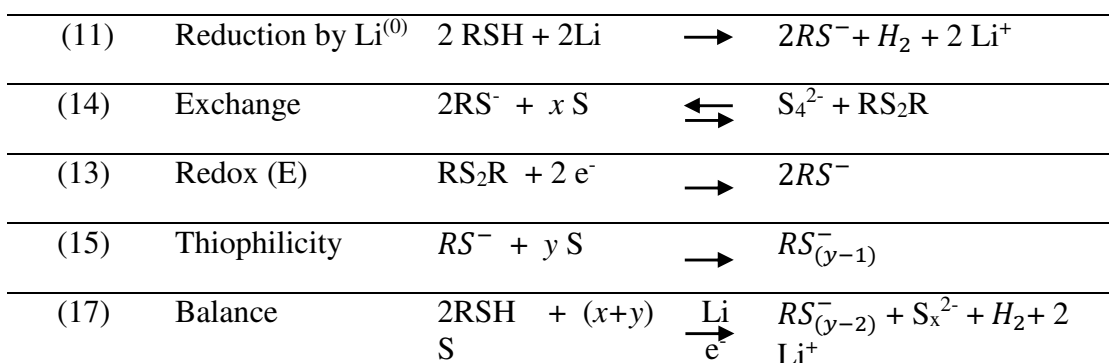


Figure 2. Discharge profile of C/S cathode in presence of organic thiol or disulphide (cycle 1 and cycle 20) at C/10 for the cells with catholyte containing 0.2 mol.L⁻¹ of (a) BTFBT, (b) DMDO and (c) Ph₂S₂. (d) Comparison of the 20th discharge cycle of all the catholytes compared to reference electrolyte without additive (dashed curve).

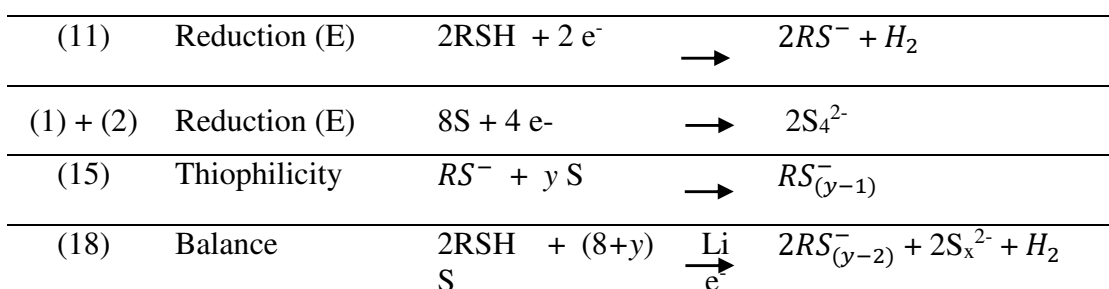
At the discharge, in the case of BTFBT, the new plateau P3 is located at high potential (2.51 V). For ease of visualization, only the discharge curves for the 20th cycle are superimposed and compared the cell without reference electrolyte in Figure 2d. (P1, R1, R2 and P2) which also retain their respective capacities (Figure 2a). With diphenyl disulphide (Figure 2c), P3 (~ 2.25V) appears at lower potential than P1 (2.35V) which is extremely reduced. The other 3 regions R1, R2 and P2 are preserved. Finally, in the case of DMDO shown in Figure 2b, the first discharge cycle corresponds to the only plateau P2 that is conserved to the charge (in oxidation). The curves are also very different from each other with two distinct trays clearly defined for BTFBT corresponding to successive non-competitive oxidation step of the mineral polysulfide S_x^{2-} and organic RS_y^- ions. Whereas in the other two cases Ph₂S₂ or DMDO only one oxidation plateau is observed.

After 20 cycles, the discharge curves show that in the case of the two thiols, the first part of the discharge curve of the mineral sulphur is strongly affected (P1, R1) while the second part is less disturbed. In the case of diphenyl disulphide, the two regions have the same pace with a smaller decrease in capacity which is more pronounced on the second plateau. The superposition of the discharge curves at the 20th cycle for the 4 cells (with and without additive) (Figure 2d) clearly shows the distinction between the shape of the curves corresponding to the difference in reactivity between the alkyl (DMDO) and aryl systems, polysulfides (BTFBT, Ph₂S₂) with sulphur or polysulfide ions.

First, the dithiol DMDO very easily reducible as expected by the LUMO orbitals values, and the S partial charge of thiolate (Table 4), is instantly converted into dithiolate in the presence of lithium metal as soon as it is added to the cell before sealing it²⁸. $(\text{CH}_2\text{O}(\text{CH}_2)_2\text{S}^-)_2$ reacts later instantly with the sulphur of the cathode (Eq. 14 and Eq. 15), thereby initiating the chemical reduction of sulphur, which explains the total absence of first sulphur reduction step (P1 and R1) on discharge curve (Figure 2b). The electrochemical reduction of disulphide generated in exchange reaction Eq. 14, is visible in plateau P3 at 2.25V. These successive and competitive reactions lead to the balance 17 in the case of DMDO. Consequently, the discharge curve in this case begins with the direct reduction of polysulfide ions S_4^{2-} on the P2 plateau according to the balance (17).



With BTFBT, the reduction of thiol by lithium metal is less easy. Its electrochemical reduction is initiated on P3, and precedes that of the sulphur reduction plateau P1. When the thiolate ion has a strong charge delocalisation, as in this case due to the presence of two CF_3 groups, it is less reactive. Its exchange reactions with sulphur (Eq. 13 and 15) are less favoured thermodynamically and kinetically slower. As a result, a large part of the sulphur is electrochemically accessible and there is the superposition of the plateau P3 followed by P1 and R1.



The diphenyl disulphide presents as shown in Table 2, an intermediate position in terms of thiolate ion stability. Its electrochemical reduction is then concomitant with the first step of sulphur reduction, we observe by consequence, a single plateau which is a sum of P3 and P1. Sulphur exchange reactions are limited for phenylthiolate at single S—S bond (i.e. PhS_2^-). Its partial oxidation by the polysulfide ions formed (Eq. 14) limits their diffusion and own electrochemical reduction. It can thus be said that the catalytic reduction of sulphur in the presence of thiolates is more or less stabilized $(\text{CF}_3)_2\text{PhS}^- > \text{PhS}^- > (\text{CH}_2\text{O}(\text{CH}_2)_2\text{S}^-)_2$ reduces the risk of successive uncontrolled reductions of sulphur and therefore constitute an effective chemical barrier to the redox shuttle phenomena of the LiS battery.

Table 5. Theoretical and experimental normalized capacities, discharge voltage (V), energy efficiency (%) and capacity retention (up to cycle 20) for cells with standard electrolyte (no additive) and the catholytes (BTFBT, DMDO and Ph_2S_2) from galvanostatic cycling at C/5 or C/10 as specified.

Catholyte / Electrolyte	Normalized C_D^{th} (mAh.g ⁻¹)	C_D^{exp} cycle 20 (mAh.g ⁻¹)	U_{dis} (V)	C (ret) (%)	$\eta(E)$ (%) C/5
Ref	1675	744	2.09	44.1	89.8
BTFBT	2086	1634	2.23	78.3	93.9
DMDO	2280	1810	2.10	79.4	96.9
Ph_2S_2	2508	2280	2.17	90.9	96.0

In each studied catholyte, the oxidation step of organic and inorganic polysulfide ions mixture deposits on the electrode a large part of sulphur as the organic RS_xR and mineral S compounds. We cannot rule out that a part of these species remains after oxidation in solution (within the limit of solubility of these compounds). The appearance of cycle 20 and the performances which includes the obtained capacity retention, percentage irreversible (C_D/C_C), nominal discharge voltage and energy efficiency are summarized in Table 5. These results show in all cases, that the total experimental capacity obtained is close to 80% of the theoretical capacity. They also indicate a higher energy efficiency of the BTFBT because of its high nominal potential.

Since the reduction potential of the organic sulphide species is higher than the higher capacity reaction P2 of the mineral sulphur, the addition of the catholyte tends to increase the nominal discharge voltage. An increased discharge voltage is better for improving the energy density of the system. The average discharge voltage calculated by dividing the discharge energy

(mWh) by the discharge capacity (mAh) is summarized for the electrolytes and catholytes in Table 5. It can be seen that this voltage value is the highest in case of BTFBT, due to the existence of the P3 in this case at the relatively highest potential (~2.51 V). The cells with DMDO and Ph₂S₂ catholytes have intermediate discharge voltage followed by the cell with the standard electrolyte.

4.2. Effect of kinetics on Voltage Profile at high current density (C/5)

A comparison of the charge and discharge voltage profiles at C/5 (2nd cycle) for catholytes containing BTFBT, DMDO and PH₂S₂ is shown in Figure 2 (a), (b) and (c) respectively. For comparison, a typical charge/discharge curve from a cell containing the standard electrolyte (no additive) is also shown (dashed curve). In the case of BTFBT, the redox reaction in P3 additional plateau (P3) for the additive are easier and more precisely observed in the corresponding dQ/dV curves showed in Figure 2d. We can show that for BTFBT, P3 is highly reversible ($\Delta V \sim 20$ mV) and distinct from P1. For DMDO and PH₂S₂, P1 and P3 are closer together with also very reversible system of 19 mV and 29 mV respectively.

Furthermore, in presence of BTFBT, the two standard plateaus corresponding to the reduction of mineral sulphur (P1: 388 mAh.g⁻¹) and (P2: 779 mAh.g⁻¹) are also observed during the discharge at the expected potential by comparison without BTFBT, in the same conditions the discharge profile shown (P1: 251 mAh.g⁻¹) and (P2: 515 mAh.g⁻¹). In both cases the R2 region is absent, which means that the S₂²⁻ ions do not have time to form. In other words, the equilibrium 10, table 2, is too slow by comparison of the diffusion of the S²⁻ ions. This remark can also be applied to (PhS)₂ figure 2c, whereas for DMDO, a small plate at the end of the discharge curve indicates the formation of the small quantity of S²⁻ ion (fig 2b).

As we explained previously, the ratio $r = \frac{P_2}{(P_1 + R_1)}$ is indicative of thermodynamic displacement (K_i) of exchange and dissociation equilibria (5 to 9 table 2) that follows the electrochemical process. While, their absolute value of P1, P2 indicate the amount of sulphur active in the redox/chemical process i.e. rate of evolution of the chemical reactions (ki). Ideally, by controlling thermodynamic and kinetic parameters, the ratio is $r = 2$, and absolute values are $P_2 = 2P_1 = 800$ mAh.g⁻¹. In fact, the changing value of r and P1, P2 the more the discharge regime (formation time of the polysulfide ions) is incompatible with their chemical reaction rate and equilibria, they then have time to diffuse and reduce. It is for this reason that it is difficult to maintain the good performance at high discharge regime for LiS batteries.

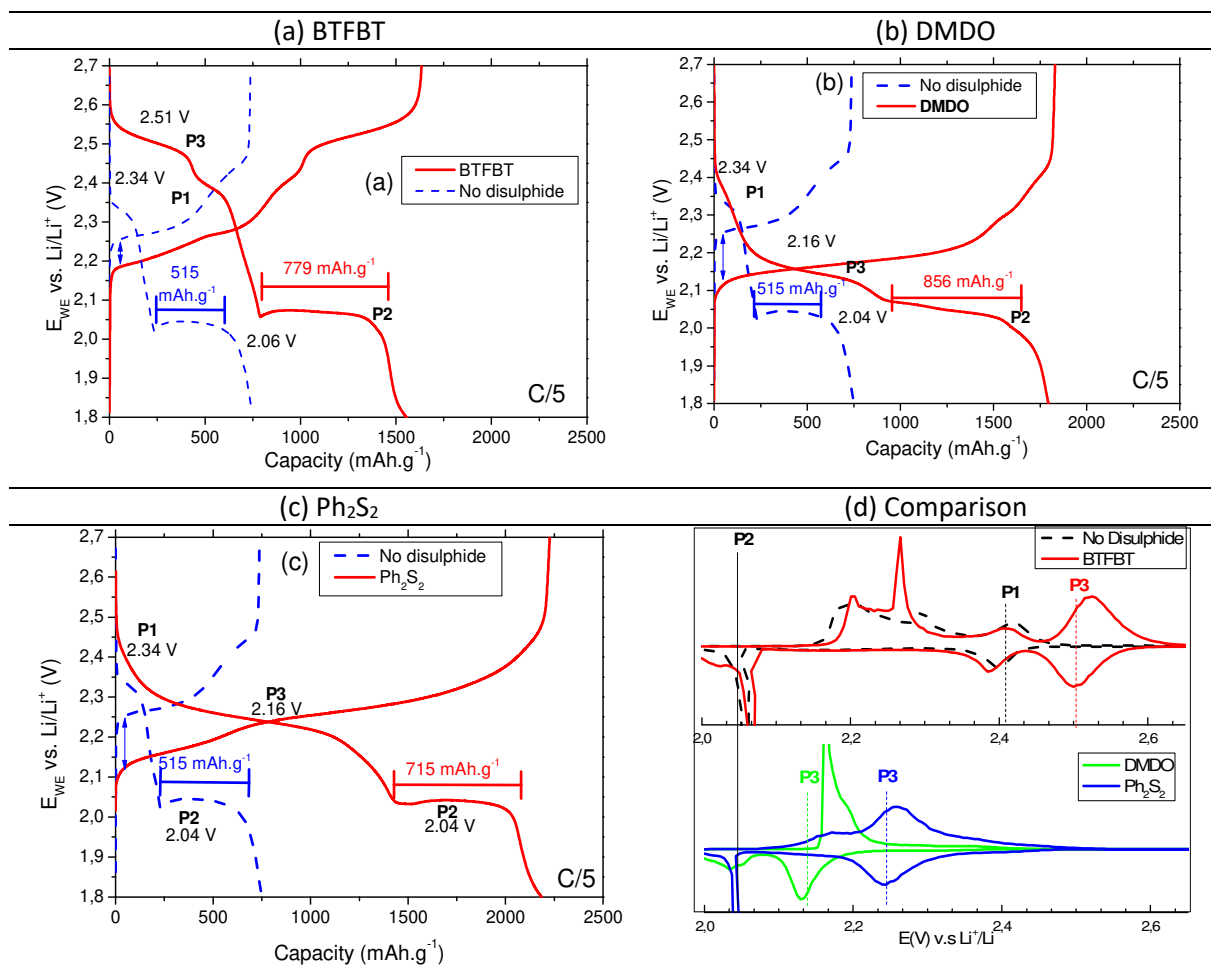


Figure 3. Voltage profiles under galvanostatic cycling at C/5 for cells containing standard electrolyte (DOL/DME + 0.75 M LITFSI + 0.25 M LiNO₃) without (dashed curve) and with (a) 0.2 M BTFBT, (b) 0.2 M DMDO, (c) 0.2 M Ph₂S₂, and (d) corresponding dQ/dV curves

It is interesting to note that the ratio r is close to 2 for all cases with and without additive. While the absolute capacity values corresponding to P2 are in order (DMDO > BTFBT > (PhS)₂ > ref). This indicates that the presence of the catholyte plays a role in extracting a larger fraction of the theoretical effective capacity of P2 (800 mAh.g⁻¹). At C/5, the total initial capacity obtained in the standard electrolyte is 749 mAh.g⁻¹, while in the BTFBT catholyte it is 1556 mAh.g⁻¹. If we subtract the capacity corresponding to P3 (455 mAh.g⁻¹), we can estimate the capacity from mineral sulphur only, which is 1101 mAh.g⁻¹. By a similar calculation, the capacity of mineral sulphur in the presence of the DMDO catholyte is estimated to be 1016 mAh.g⁻¹. In the case of Ph₂S₂, the P1 plateau is not distinctly observed, which makes the estimation difficult. Recalling that the effective reversible capacity (without formation of S²⁻ in region R2) is 1200 mAh.g⁻¹, we can say that in the presence of thiol or organic

disulphide up to 92 % of this capacity is obtained while only 62% of the sulphur is reduced reversible without at C/5. It is however, clear that in presence of the catholyte results in an approximately 33% higher sulphur utilization at C/5.

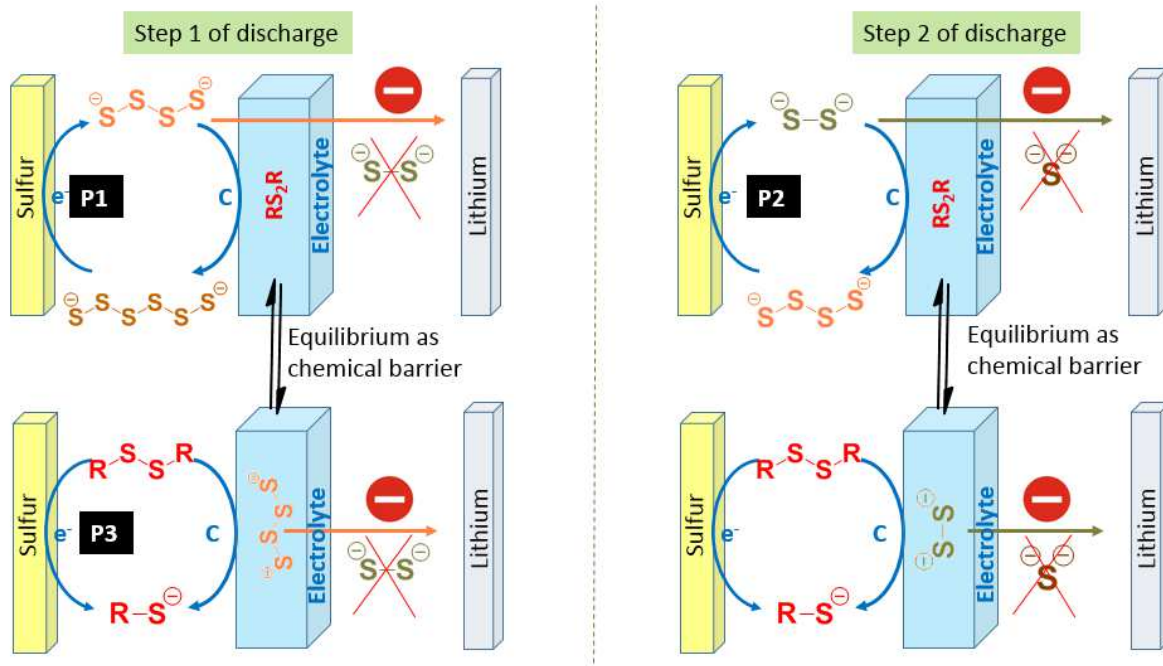
Also noteworthy is the impact of the presence of additives on the charging overpotential. (voltage difference between the charge curve in the presence of organic sulphide (solid curve) and in the absence of (dashed curve) as shown in Figure 2 (a to c). The onset potential for oxidation is approximately 70 mV, 110 mV and 130 mV lower in case of BTFBT, DMDO and Ph₂S₂ respectively. This is due to a catalytic effect of the sulphur redox processes in the presence of thiolates. The reduction of charging potential benefits the energy efficiency as listed in Table 5. The calculated energy efficiency in the standard electrolyte (89.8%) is comparable to commercial Li-ion batteries [55-57], whereas in presence of the additive it increases by another (4% to 7%).

In conclusion of this part we can say that the addition of thiol or disulphide in the electrolyte acts in a similar way via the thiolate ions in solution. Its benefit is visible at the two key stages of sulphur reduction as follows:

- It slows down the diffusion of the S₄²⁻ polysulfide ions and their simultaneous reduction at the electrode during the processes (P₁ + R₁).
- It blocks the formation of S²⁻ ions responsible for the loss of sulphur by Li₂S precipitation during steps (P₂ + R₂).

These effects are illustrated in Scheme 1, which shows in the step 1 of discharge (P₁+ R₁ +P₃) that the presence of equilibrium between the RS₂R and S₄²⁻ maintains a homogeneous solution and forms a barrier against their diffusion and evolution in solutions. This benefit is independent of the fact that the reduction of the additive (P₃) precedes, is simultaneous, or succeeds that of the sulphur P₁. In the second discharge step, the kinetic chemical equilibrium favoured in the presence of thiolate / disulphide system forms a barrier against the formation of strongly reducing ions S²⁻ and optimizes the use of sulphur at high speed.

For all systems studied we have also characterized of the rate performance at different C-rate, the results are summarized in figure S1 (in supporting information). These results demonstrate a similar behaviour of the four systems, the organic additive does not modify their rate performance by comparison with standard electrolyte.



Schema 1. Illustration of the mechanism for beneficial action of disulphide (or thiol) additive as a chemical barrier to prevent the harmful evolution during the two successive stages of sulphur reduction.

4.3. Stability of Lithium/Catholyte Interface

Most aprotic electrolytes are not stable against metallic lithium, resulting in a solid electrolyte interface (SEI) on the lithium anode. [22, 58, 59]. During the cycling, such SEI layer breaks and reforms due to the volume change and lithium dendrite, which consumes a lot of electrolytes and lithium and causes low Coulombic efficiency as well. In Li-S batteries, the shuttle effect brings about more parasitic reactions, making the formation of stable SEI more difficult than in Li-ion batteries. In early work [59], we have shown that LiNO_3 significantly improves the cycling efficiency of Li metal on the Li surface in PS solution (i.e., in catholyte-B) by participating in the formation of a stable passivation film. [60] However, the effect of formed organic polysulphides RS_y^- ($y = 1$ to 5) on the Li-anode cannot be neglected. To address this, in the present work, we study the Li stripping/deposition on the relevant catholyte in symmetric Li cells. Thanks to intermediate reactivity of Ph_2S_2 , we chose to focus on its effect on lithium surface modification by comparison with standard electrolyte. A current density of $0.4 \text{ mA}\cdot\text{cm}^{-2}$ was used, with reversal of current direction every 20 minutes.

Overall, the cells were run for 70 h and after completion of the experiment the surface of the cycled Li disk was observed under SEM.

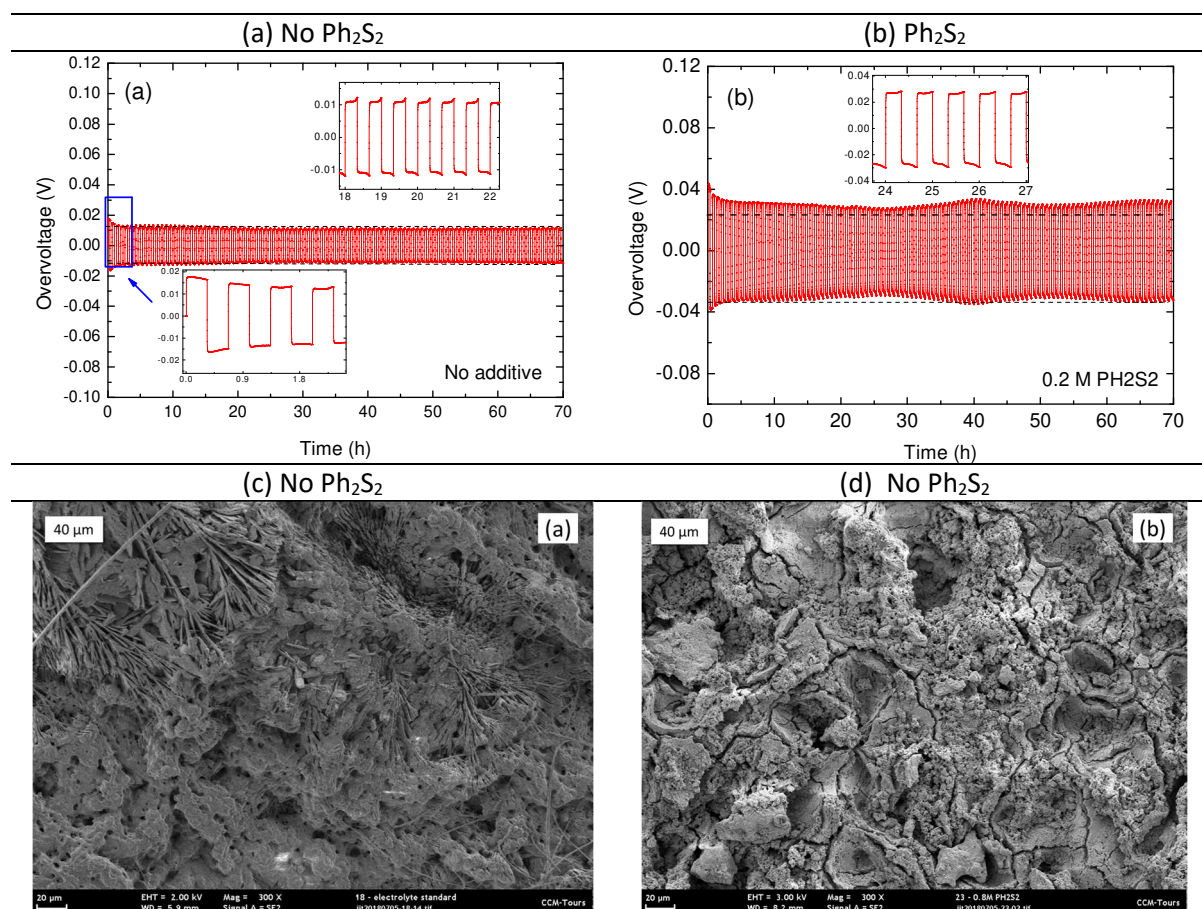


Figure 4. 70 h of stripping/deposition and corresponding Li surface SEM images in symmetric Lithium cells using (a, c) standard electrolyte (no additive) and (b, d) 0.2 M Ph_2S_2 catholyte.

The results from the stripping/deposition measurement are shown in Figure 3 (a) and (b) for the standard electrolyte and the Ph_2S_2 catholyte respectively. In the standard electrolyte the overvoltage is ~ 13 mV and is relatively constant throughout the 70 h of test. In the inset showing the start of the cycling, it can be seen that the overvoltage decreases from an initial value of 18 mV which can be ascribed to the removal of surface contaminants. By comparison, in the catholyte the average overvoltage is approximately 250% higher at ~ 32 mV. A part of the increase in overvoltage may be due to the difference in conductivity of the two electrolytes. The presence of the Ph_2S_2 additive increases the viscosity of the electrolyte [30], thus reducing the conductivity. Our conductivity measurements showed that the conductivity of the standard electrolyte ($10.2 \text{ mS}\cdot\text{cm}^{-1}$, 25°C) is only 20% higher than the

catholyte ($8.2 \text{ mS}\cdot\text{cm}^{-1}$, 25°C). [44] Therefore, it appears that most of increased overvoltage is due to the presence of the additional layer formed on the lithium due to deposited products. Additionally, it can also be seen in Figure 3 (b) that the overvoltage cyclically increases and decreases during the test indicating that the surface is undergoing continuous modification.

These observations are in good agreement with the observed SEM images in Figure 3 (c, d), Indeed the observed surface are entirely different and continuous coating on the lithium can be observed in presence of additive. In the absence of the additive (Figure 3 (a)), the surface of the lithium exhibits surface characteristics similar to those described in literature as “spongy lithium” [61]. When the additive is present in the electrolyte, the lithium anode cannot be observed directly as the surface appears to be covered by a thick layer of deposits. It is possible deposit majorly consists of Li^+RS^- which is the product of the chemical reaction of the of the disulphides and Li. The existence of such a passivation layer would prohibit further reaction of Lithium with the organic disulphide and could explain the good coulombic efficiency obtained on long cycling discussed in the next paragraph. From these results, we can conclude that the relative lower overvoltage of a good passivation layer observed in presence of PhS_2Ph allows the lithium to be used in the Li//S cell without any significant impact on the discharge and charge voltage even at high c-rates (1C).

4.4. Long term cycling

The effect of addition of the catholytes (Ph_2S_2 and BTFBT) during long cycling was evaluated by cycling the cells at 1C rate. The obtained results are shown in Figure 4 and compared with the cell containing the standard electrolyte (no additive). Galvanostatic profile (figure 4a) for BTFBT and standard electrolyte for are compared at all 100 cycles. Evolution of capacities as function of cycles, as well as calculated capacity fade rates by linear fitting are mentioned in the graph figure 4c. At this fast regime, the kinetic control of chemical balance (5 to 10, table 2) and (14, 15 table 3) is even more marked. It differentiates the behaviour of the three electrolytes as well by the initial value of capacity as by its decrease throughout the cycling. It can be seen that the initial capacity follows the following order (Ph_2S_2) > (BTFBT) > (Standard - no additive). The increase in capacity is a combined effect of the added capacity due to the catholyte as well as the additional capacity obtained from the redox reaction of the mineral sulphur in presence of the additives.

At high cycling speed (C-rate) the competition between chemical equilibria concerning mineral polysulphides S_x^{2-} (eq 5 to eq 10) and chemical equilibria between the mineral

polysulfide ions and the organic additives (14 and 15), is in favour of these latter. Thus, the most reactive thiolate (DMDO) favours the highest initial capacity. At the same time, the most reactive thiolate ion favours high-rank organic polysulfide ions RS_y^- ($y = 3, 4$) (eq 15 Table 3) and their oxidation to high rank RS_zR polysulfanes ($z > 2$) (eq. 16, table 3). RS_3R and RS_4R are less soluble and will be responsible for the progressive loss of active disulphides and sulphur.

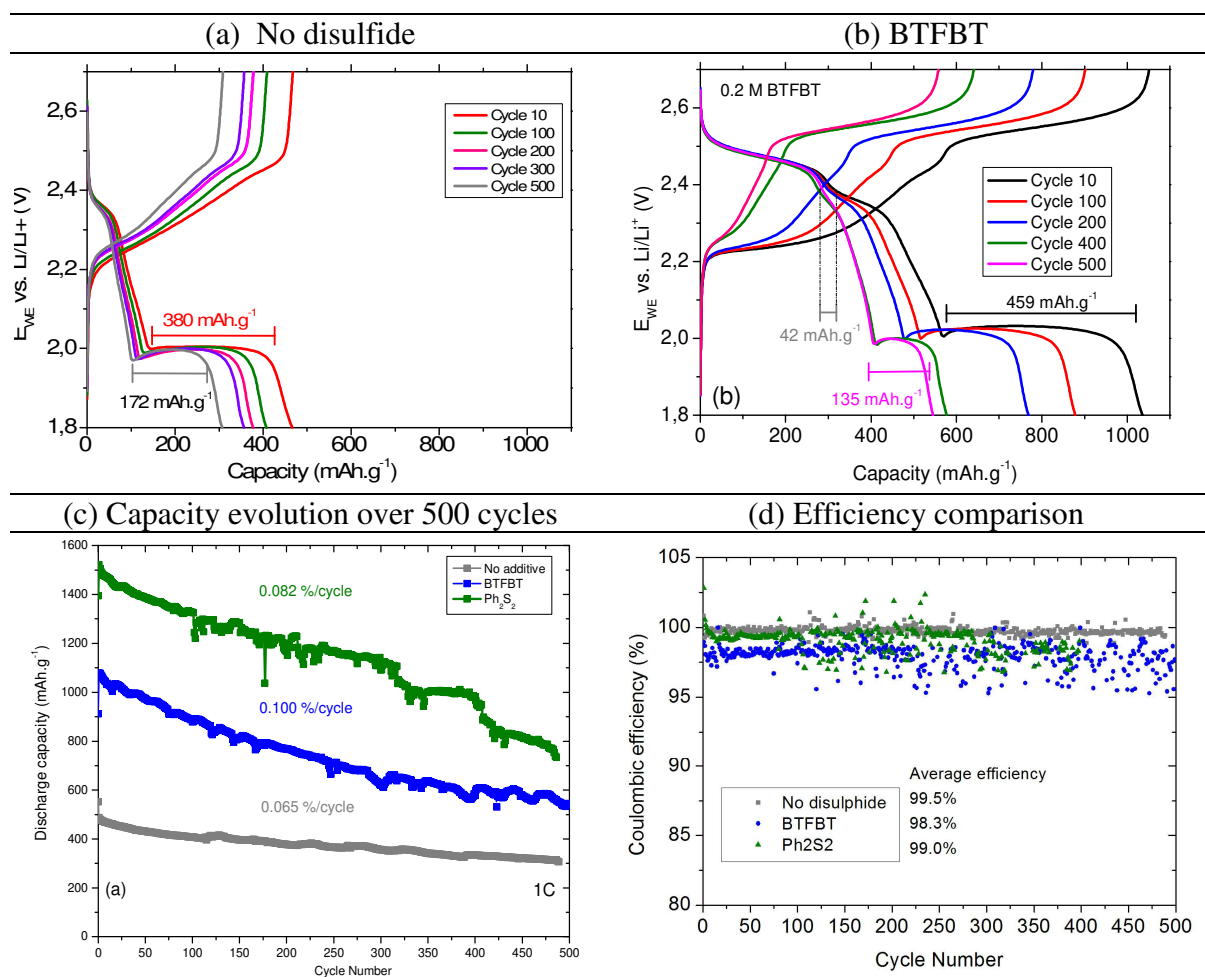


Figure 5. Galvanostatic potential profiles for the cell containing 0.2 M BTFBT (cycle number 10, 100, 200, 400 and 500 for cells at 1C rate containing no additive (a), 0.2 M BTFBT (b). Comparison of capacity evolution (c) and efficiency (d) for long-term cycling.

These considerations can be explained why DMDO catholyte showed poor capacity retention over long cycling even its initial capacity is better, and hence has not been shown. While, the capacity fade rate calculated over 500 cycles is the lowest for the standard electrolyte (0.065

%/cycle) as compared to the Ph_2S_2 electrolyte (0.082 %/cycle) and the BTFBT electrolyte (0.082 %/cycle).

The galvanostatic profiles for BTFBT (figure 4 a) compared to the standard electrolyte (Figure 4b) confirm that $(\text{CF}_3)_2\text{PhS}^-$ is stable thiolate and allow reversible redox system. Its capacity (P3) close 300 mAh.g^{-1} is invariable over cycling. While the capacity obtained from the P2 plateau corresponding to second step of reduction for mineral polysulphides initially close to 459 mAh.g^{-1} decreases rapidly. A slightly lower discharge capacity (403 mAh.g^{-1}) of the P2 plateau was observed with the Ph_2S_2 (no showed herein). By comparison, the capacity of the P2 plateau in the cell with standard electrolyte is much lower at 335 mAh.g^{-1} implying that the presence of the catholyte has the additional effect on increasing the capacity utilization of redox of the mineral sulphur.

Throughout the cycling, at this current density (fast kinetic), this protection decreases and there is a gradual decrease of the plateau P2. This means that the S_4^{2-} react chemically with the RS_2R (eq 8 to 10) and are no longer electrochemically active. In other words, the chemical equilibrium of exchange (eq 14, table 3) is too fast by comparison of the electronic transfer of the redox process (eq 3, table 1). Especially because, during cycling the surface of the cathode becomes less conductive due to anarchic deposition of insulating sulphur. This is partly evidenced by the fact that at the end of the cycling, the remaining capacity from the P2 plateau of mineral sulphur is only 136 mAh.g^{-1} (Figure 4b). By comparison, in the cell with the standard electrolyte the capacity retention appears to be much higher with a remaining capacity for P2 of 206 mAh.g^{-1} . Over the course of 500 cycles, the addition of the electrochemically active catholytes leads to a higher capacity utilization of the mineral sulphur, enhancement of the total capacity, slight lowering of the capacity fade rate depending to the nature of organic compound while maintaining a high coulombic efficiency $\eta \geq 97 \%$ (Figure 4d).

Conclusion

In this study, we have shown that during cycling of the S/C cathode, the addition of thiol or disulphide in the standard electrolyte DOL/DME + LiTFSI/LiNO₃ acts via the reactivity of the thiolate ions. It serves as chemical barrier in solution toward the S_4^{2-} polysulfide ions diffusion and their simultaneous reduction. All their harmful consequence on performance are then reduced thanks to the kinetic (redox process, diffusion) and thermodynamic (exchange, thiophilicity, disproportionation) control of more than 17 reactions between the $\text{RS}_2\text{R}/\text{RS}^-$ and

S/S₄²⁻ systems. It maintains a homogeneous solution and forms a barrier against their diffusion and evolution in solutions. The link between the displacement of these equilibria and the relative stability of the formed polysulfide ions RS_y⁻ according to their chemical structure and the electronic effects allow the classification of their relative effectiveness as BTFBT > Ph₂S₂ > DMDO. At high cycling C-rate the competition between chemical equilibria of S_x²⁻ following their redox formation and their reactivity with the organic additives is in favour of the stabilisation of high order polysulphides S_x²⁻ (x > 4). The most reactive dithiolate (DMDO) favours the highest initial cumulated capacity. However, the most reactive thiolate ion favours high-rank organic polysulfide ions RS_y⁻ (y = 3, 4) and their consecutive oxidation to less soluble RS_zR polysulfanes (z > 2). This feature will be responsible for the progressive loss of active disulphides and sulphur and then capacity at long-term cycling at C-rate.

Finally, lithium anode stripping and galvanostatic cycling at slower C/10-rate, demonstrate effective protection of lithium and catalytic reduction of sulphur in the presence of stable thiolates (CF₃)₂PhS⁻ > PhS⁻ > (CH₂O(CH₂)₂S⁻)₂. The consequence of this new approach is at the same time reduces the risk of successive uncontrolled reductions of sulphur and therefore constitute an effective chemical barrier to the redox shuttle phenomena of the LiS battery. By insisting on the very complex reaction mechanism, this study has shown that the original formulation of an effective organosulfur catholyte consists on kinetic and thermodynamic control of their reactivity with the polysulfide ions in solution by controlling their chemical structure.

Acknowledgements

The authors would like to thank “Le Studium Loire Valley Institute for Advanced Studies” for financial support to researchers involved in this study under Lavoisier regional program. We would also like to thank Dr. Pierre-Yvon Raynal at Faculty of Medicine in Tours for SEM characterization of samples.

References

[1] B. Nykvist, M. Nilsson, Rapidly falling costs of battery packs for electric vehicles, *Nature Climate Change*, 5 (2015) 329.

- [2] J. Neubauer, E. Wood, The impact of range anxiety and home, workplace, and public charging infrastructure on simulated battery electric vehicle lifetime utility, *J. Power Sources*, 257 (2014) 12-20.
- [3] A. Manthiram, Y. Fu, S.-H. Chung, C. Zu, Y.-S. Su, Rechargeable Lithium–Sulfur Batteries, *Chemical Reviews*, 114 (2014) 11751-11787.
- [4] J. Scheers, S. Fantini, P. Johansson, A review of electrolytes for lithium–sulphur batteries, *J. Power Sources*, 255 (2014) 204-218.
- [5] D. Bresser, S. Passerini, B. Scrosati, Recent progress and remaining challenges in sulfur-based lithium secondary batteries – a review, *Chemical Communications*, 49 (2013) 10545-10562.
- [6] S. Evers, L.F. Nazar, New Approaches for High Energy Density Lithium–Sulfur Battery Cathodes, *Accounts of Chemical Research*, 46 (2013) 1135-1143.
- [7] K. Xie, Y. You, K. Yuan, W. Lu, K. Zhang, F. Xu, M. Ye, S. Ke, C. Shen, X. Zeng, X. Fan, B. Wei, Ferroelectric-Enhanced Polysulfide Trapping for Lithium–Sulfur Battery Improvement, *Advanced Materials*, 29 (2017) 1604724.
- [8] H. Al Salem, G. Babu, C. V. Rao, L.M.R. Arava, Electrocatalytic Polysulfide Traps for Controlling Redox Shuttle Process of Li–S Batteries, *Journal of the American Chemical Society*, 137 (2015) 11542-11545.
- [9] W. Hua, Z. Yang, H. Nie, Z. Li, J. Yang, Z. Guo, C. Ruan, X.a. Chen, S. Huang, Polysulfide-Scission Reagents for the Suppression of the Shuttle Effect in Lithium–Sulfur Batteries, *ACS Nano*, 11 (2017) 2209-2218.
- [10] M. Chen, S. Zhao, S. Jiang, C. Huang, X. Wang, Z. Yang, K. Xiang, Y. Zhang, Suppressing the Polysulfide Shuttle Effect by Heteroatom-Doping for High-Performance Lithium–Sulfur Batteries, *ACS Sustainable Chemistry & Engineering*, 6 (2018) 7545-7557.
- [11] J. Liu, D. Lu, J. Zheng, P. Yan, B. Wang, X. Sun, Y. Shao, C. Wang, J. Xiao, J.-G. Zhang, J. Liu, Minimizing Polysulfide Shuttle Effect in Lithium-Ion Sulfur Batteries by Anode Surface Passivation, *ACS Applied Materials & Interfaces*, 10 (2018) 21965-21972.
- [12] A.N. Mistry, P.P. Mukherjee, “Shuttle” in Polysulfide Shuttle: Friend or Foe?, *The Journal of Physical Chemistry C*, 122 (2018) 23845-23851.
- [13] H. Yao, G. Zheng, W. Li, M.T. McDowell, Z. Seh, N. Liu, Z. Lu, Y. Cui, Crab Shells as Sustainable Templates from Nature for Nanostructured Battery Electrodes, *Nano Letters*, 13 (2013) 3385-3390.
- [14] G. Zheng, Y. Yang, J.J. Cha, S.S. Hong, Y. Cui, Hollow Carbon Nanofiber-Encapsulated Sulfur Cathodes for High Specific Capacity Rechargeable Lithium Batteries, *Nano Letters*, 11 (2011) 4462-4467.
- [15] N. Jayaprakash, J. Shen, S.S. Moganty, A. Corona, L.A. Archer, Porous Hollow Carbon@Sulfur Composites for High-Power Lithium–Sulfur Batteries, *Angewandte Chemie International Edition*, 50 (2011) 5904-5908.

- [16] W. Li, G. Zheng, Y. Yang, Z.W. Seh, N. Liu, Y. Cui, High-performance hollow sulfur nanostructured battery cathode through a scalable, room temperature, one-step, bottom-up approach, *Proceedings of the National Academy of Sciences*, 110 (2013) 7148-7153.
- [17] J. Guo, Y. Xu, C. Wang, Sulfur-Impregnated Disordered Carbon Nanotubes Cathode for Lithium–Sulfur Batteries, *Nano Letters*, 11 (2011) 4288-4294.
- [18] L. Suo, Y.-S. Hu, H. Li, M. Armand, L. Chen, A new class of Solvent-in-Salt electrolyte for high-energy rechargeable metallic lithium batteries, *Nature Communications*, 4 (2013) 1481.
- [19] C. Davis III, J.C. Nino, Microwave Processing for Improved Ionic Conductivity in Li₂O–Al₂O₃–TiO₂–P₂O₅ Glass-Ceramics, *Journal of the American Ceramic Society*, 98 (2015) 2422-2427.
- [20] M. Nagao, A. Hayashi, M. Tatsumisago, Fabrication of favorable interface between sulfide solid electrolyte and Li metal electrode for bulk-type solid-state Li/S battery, *Electrochemistry Communications*, 22 (2012) 177-180.
- [21] G. Li, Z. Li, B. Zhang, Z. Lin, Developments of Electrolyte Systems for Lithium–Sulfur Batteries: A Review, *Frontiers in Energy Research*, 3 (2015).
- [22] H. Yang, A. Naveed, Q. Li, C. Guo, J. Chen, J. Lei, J. Yang, Y. Nuli, J. Wang, Lithium sulfur batteries with compatible electrolyte both for stable cathode and dendrite-free anode, *Energy Storage Materials*, 15 (2018) 299-307.
- [23] H. Kang, M. Boyer, G.S. Hwang, J.-w. Lee, Lithium-coated carbon cloth for anode of Lithium rechargeable batteries with enhanced cycling stability, *Electrochimica Acta*, 303 (2019) 78-84.
- [24] M. Li, X. Liu, Q. Li, Z. Jin, W. Wang, A. Wang, Y. Huang, Y. Yang, P4S10 modified lithium anode for enhanced performance of lithium–sulfur batteries, *Journal of Energy Chemistry*, (2019).
- [25] G. Ma, Z. Wen, J. Jin, M. Wu, G. zhang, X. Wu, J. Zhang, The enhanced performance of Li–S battery with P14YRTFSI-modified electrolyte, *Solid State Ionics*, 262 (2014) 174-178.
- [26] M. Barghamadi, A.S. Best, A.F. Hollenkamp, P. Mahon, M. Musameh, T. R  ther, Optimising the concentration of LiNO₃ additive in C4mpyr-TFSI electrolyte-based Li-S battery, *Electrochimica Acta*, 222 (2016) 257-263.
- [27] J. Zheng, X. Fan, G. Ji, H. Wang, S. Hou, K.C. DeMella, S.R. Raghavan, J. Wang, K. Xu, C. Wang, Manipulating electrolyte and solid electrolyte interphase to enable safe and efficient Li-S batteries, *Nano Energy*, 50 (2018) 431-440.
- [28] M. Liu, X. Chen, C. Chen, T. Ma, T. Huang, A. Yu, Dithiothreitol as a promising electrolyte additive to suppress the “shuttle effect” by slicing the disulfide bonds of polysulfides in lithium-sulfur batteries, *J. Power Sources*, 424 (2019) 254-260.
- [29] T. Mukra, Y. Horowitz, I. Shekhtman, M. Goor, S. Drvari   Talian, L. Burstein, J. Kasnatscheew, P. Meister, M. Gr  nebaum, M. Winter, H.-D. Wiemh  fer, D. Golodnitsky, E. Peled, Disiloxane with nitrile end groups as Co-solvent for electrolytes in lithiumsulfur batteries – A feasible approach to replace LiNO₃, *Electrochimica Acta*, 307 (2019) 76-82.

- [30] S. Phadke, E. Coadou, M. Anouti, Catholyte Formulations for High-Energy Li-S Batteries, *J. Phys. Chem. Lett.*, 8 (2017) 5907-5914.
- [31] H.-L. Wu, M. Shin, Y.-M. Liu, K.A. See, A.A. Gewirth, Thiol-based electrolyte additives for high-performance lithium-sulfur batteries, *Nano Energy*, 32 (2017) 50-58.
- [32] S. Chen, F. Dai, M.L. Gordin, Z. Yu, Y. Gao, J. Song, D. Wang, Functional Organosulfide Electrolyte Promotes an Alternate Reaction Pathway to Achieve High Performance in Lithium–Sulfur Batteries, *Angewandte Chemie International Edition*, 55 (2016) 4231-4235.
- [33] Y.V. Mikhaylik, J.R. Akridge, Polysulfide Shuttle Study in the Li/S Battery System, *Journal of The Electrochemical Society*, 151 (2004) A1969-A1976.
- [34] X. Ji, L.F. Nazar, Advances in Li–S batteries, *Journal of Materials Chemistry*, 20 (2010) 9821-9826.
- [35] Y.-S. Su, Y. Fu, T. Cochell, A. Manthiram, A strategic approach to recharging lithium-sulphur batteries for long cycle life, *Nature Communications*, 4 (2013) 2985.
- [36] R. Chen, T. Zhao, F. Wu, From a historic review to horizons beyond: lithium–sulphur batteries run on the wheels, *Chemical Communications*, 51 (2015) 18-33.
- [37] Electrochemical Reactions of Sulfur Organic Compounds, *Encyclopedia of Electrochemistry*.
- [38] A.J. Parker, N. Kharasch, The Scission Of The Sulfur-Sulfur Bond, *Chemical Reviews*, 59 (1959) 583-628.
- [39] T.B. Nguyen, Recent Advances in Organic Reactions Involving Elemental Sulfur, *Advanced Synthesis & Catalysis*, 359 (2017) 1066-1130.
- [40] J. Robert, M. Anouti, M. Abarbri, J. Paris, Nucleophilic substitution of acyl chlorides by electrogenerated polysulfide ions in N,N-dimethylacetamide, *Journal of the Chemical Society. Perkin Transactions 2*, (1997) 1759-1764.
- [41] J. Robert, M. Anouti, J. Paris, Reactivity of benzyl disulfide and thiolate ions towards activated nitrobenzenes in N,N-dimethylacetamide, *New J. Chem.*, 21 (1997) 1187-1196.
- [42] J. Robert, M. Anouti, J. Paris, Formation of acyldisulfide ions from the reaction of sulfur with thiocarboxylate ions, and reactivity towards acyl chlorides in N,N-dimethylacetamide, *Journal of the Chemical Society. Perkin Transactions 2*, (1997) 473-478.
- [43] J. Robert, M. Anouti, J. Paris, Reactivity of benzyl disulfide and thiolate ions towards activated nitrobenzenes in N,N-dimethylacetamide, *New J. Chem.*, 21 (1997) 1187-1196.
- [44] A. Ahrika, M. Anouti, J. Robert, J. Paris, Nucleophilic substitution of S-phenyl thiol esters by electrogenerated polysulfide ions in N,N-dimethylacetamide, *Journal of the Chemical Society, Perkin Transactions 2*, 0 (1998) 607-610.
- [45] M. Benaïchouche, G. Bossier, J. Paris, J. Auger, V. Plichon, Formation of stable aryldisulphide ions in dimethylacetamide from the reaction of sulphur with thiolate ions, *Journal of the Chemical Society, Perkin Transactions 2*, (1990) 31-36.

- [46] M. Benaichouche, G. Bosser, J. Paris, V. Plichon, Relative nucleophilicities of aryldisulphide and thiolate ions in dimethylacetamide estimated from their reaction rates with alkyl halides, *Journal of the Chemical Society, Perkin Transactions 2*, (1990) 1421-1424.
- [47] M. Benaichouche, G. Bosser, J. Paris, V. Plichon, Nucleophilic substitution of nitroaromatic halides by electrogenerated polysulphide ions in dimethylacetamide, *Journal of the Chemical Society, Perkin Transactions 2*, (1991) 817-823.
- [48] G. Bosser, M. Benaichouche, R. Coudert, J. Paris, Nucleophilic displacement of the nitro group of dinitrobenzenes by electrogenerated polysulfide ions in dimethylacetamide, *New J. Chem.*, 18 (1994) 511-517.
- [49] M. Liu, S.J. Visco, L.C. De Jonghe, Electrochemical Properties of Organic Disulfide/Thiolate Redox Couples, *Journal of The Electrochemical Society*, 136 (1989) 2570-2575.
- [50] G. Bosser, M. Anouti, J. Paris, Formation and scission of the sulfur-sulfur bond: a new approach to reactions between sulfur/polysulfide ions and thiolate ions/disulfides in N,N-dimethylacetamide, *Journal of the Chemical Society, Perkin Transactions 2*, 0 (1996) 1993-1999.
- [51] M.C. Verploegh, L. Donk, H.J.T. Bos, W. Drenth, Nucleophilic displacements at halogen in 1-chloro-, 1-bromo- and 1-iodo-1-alkynes: I. Thiolates as nucleophiles, *Recueil des Travaux Chimiques des Pays-Bas*, 90 (1971) 765-778.
- [52] F. Paulat, N. Lehnert, Electronic Structure of Ferric Heme Nitrosyl Complexes with Thiolate Coordination, *Inorganic Chemistry*, 46 (2007) 1547-1549.
- [53] J.E. Argüello, L.C. Schmidt, A.B. Peñeñory, "One-Pot" Two-Step Synthesis of Aryl Sulfur Compounds by Photoinduced Reactions of Thiourea Anion with Aryl Halides, *Organic Letters*, 5 (2003) 4133-4136.
- [54] P. Casuso, I. Odriozola, A. Pérez-San Vicente, I. Loinaz, G. Cabañero, H.-J. Grande, D. Dupin, Injectable and Self-Healing Dynamic Hydrogels Based on Metal(I)-Thiolate/Disulfide Exchange as Biomaterials with Tunable Mechanical Properties, *Biomacromolecules*, 16 (2015) 3552-3561.
- [55] J. Lochala, D. Liu, B. Wu, C. Robinson, J. Xiao, Research Progress toward the Practical Applications of Lithium–Sulfur Batteries, *ACS Applied Materials & Interfaces*, 9 (2017) 24407-24421.
- [56] Y. Ye, F. Wu, S. Xu, W. Qu, L. Li, R. Chen, Designing Realizable and Scalable Techniques for Practical Lithium Sulfur Batteries: A Perspective, *The Journal of Physical Chemistry Letters*, 9 (2018) 1398-1414.
- [57] S.-H. Chung, C.-H. Chang, A. Manthiram, Progress on the Critical Parameters for Lithium–Sulfur Batteries to be Practically Viable, *Advanced Functional Materials*, 28 (2018) 1801188.
- [58] Y. Guan, A. Wang, S. Liu, Q. Li, W. Wang, Y. Huang, Protecting lithium anode with LiNO₃/Al₂O₃/PVDF-coated separator for lithium-sulfur batteries, *Journal of Alloys and Compounds*, 765 (2018) 544-550.

- [59] H. Zhao, N. Deng, J. Yan, W. Kang, J. Ju, Y. Ruan, X. Wang, X. Zhuang, Q. Li, B. Cheng, A review on anode for lithium-sulfur batteries: Progress and prospects, *Chemical Engineering Journal*, 347 (2018) 343-365.
- [60] S. Li, Y. Ma, J. Ren, H. Liu, K. Zhang, Y. Zhang, X. Tang, W. Wu, C. Sun, B. Wei, Integrated, Flexible Lithium Metal Battery with Improved Mechanical and Electrochemical Cycling Stability, *ACS Applied Energy Materials*, (2019).
- [61] E. Zhao, K. Nie, X. Yu, Y.-S. Hu, F. Wang, J. Xiao, H. Li, X. Huang, Advanced Characterization Techniques in Promoting Mechanism Understanding for Lithium–Sulfur Batteries, *Advanced Functional Materials*, 28 (2018) 1707543.